Date of publication xxxx 00, 0000, date of current version xxxx 00, 0000.

Digital Object Identifier 10.1109/ACCESS.2020.DOI

Wideband Bandpass Filters Using a Novel Thick Metallization Technology

CELIA GOMEZ-MOLINA*[1], ALEJANDRO PONS-ABENZA*[1], (Student Member, IEEE), JAMES DO[2], FERNANDO QUESADA-PEREIRA[1], (Member, IEEE), XIAOGUANG LIU[2], (Senior Member, IEEE), JUAN SEBASTIAN GOMEZ-DIAZ[2], (Senior Member, IEEE), and ALEJANDRO ALVAREZ-MELCON[3], (Senior Member, IEEE)

[1]Department of Information Technologies and Communications, Universidad Politécnica de Cartagena, 30202 Cartagena, Spain. (email: {celia.gomez, alejandro.alvarez}@upct.es)

[2]Department of Electrical and Computer Engineering, University of California, Davis, USA. (e-mail: {lxgliu, jsgomez}@ucdavis.edu)

Corresponding author: Celia Gomez-Molina (e-mail: celia.gomez@upct.es).

This work is supported in part by the National Science Foundation with CAREER Grant No. ECCS-1749177, and by the Spanish Government, Ministerio de Educación, Cultura y Deporte with Ref. FPU15/02883, and the Ministerio de Economía y Competitividad through the coordinated project with Ref. TEC2016-75934-C4-R and PRX18/00092.

*Both authors contributed equally to this manuscript.

ABSTRACT A new class of wideband bandpass filters based on using thick metallic bars as microwave resonators is presented in this work. These bars provide a series of advantages over fully planar printed technologies, including higher coupling levels between resonators, higher unloaded quality factors Q_U, and larger bandwidths implemented with compact structures. In comparison to dielectric and waveguide resonators filters, higher bandwidths together with lower weight and footprint reduction are achieved with the proposed thick bars technology. Moreover, thick bar resonators can easily be coupled to an additional resonance excited in a box used for shielding, allowing to realize transversal topologies able to implement transmission zeros at desired frequencies. To illustrate the capabilities of this technology, three microwave filters with different topologies have been designed. One of the designed filters has been manufactured and tested using copper bars inside an aluminum housing partially filled with Teflon. Measured data demonstrates a fractional bandwidth of $FBW = 32\%$, spurious free range $SFR > 50\%$, unloaded quality factor of $Q_U = 1180$, insertion losses over 0.16 dB and return losses over 20 dB, without requiring any post-tuning operation on the prototype. This result confirms the exciting performance of the proposed technology for wideband applications.

INDEX TERMS Hybrid waveguide microstrip technology, microwave filters, resonator filters, transmission zeros, transversal filters, wideband filters.

I. INTRODUCTION

WIDEBAND filters are required in modern communication systems, including wireless communications, 5G, satellites, or in artificial intelligence platforms. Most of these applications require compact solutions for filters, with good performance in terms of insertion losses (IL), return losses (RL) and unloaded quality factors (Q_U).

In applications where the footprint and volume are critical, planar technologies, such as microstrip [1], [2], stripline [3] or coplanar [4], [5] are usually employed. Using these technologies, the level of losses is normally sacrificed in order to produce structures with reduced dimensions and low weight.

Among the planar solutions, microstrip technology [1] is one of the most employed in practice, due to the compactness achieved, ease of integration and low-cost fabrication. Unfortunately, the most important limitations faced by microstrip resonator filters [2] for these applications are normally small bandwidths and low Q_U. Some previous works have tried to implement broadband filters using microstrip line resonators. For instance, in [6], the authors use concentric open-loop resonators to reduce the size of the filter and achieve a fractional bandwidth $FBW \approx 10\%$. It is challenging to enhance the bandwidth of these microwave filters beyond these limits, mainly because very strong couplings are required between resonators and in the input/output (I/O) ports. However, the coupling levels achievable with microstrip line resonators are

This work is licensed under a Creative Commons Attribution 4.0 License. For more information, see https://creativecommons.org/licenses/by/4.0/.

low, which limit in practice the implementation of wideband responses. The second limiting factor of printed microstrip technology is the relatively low Q_U. This factor is typically less than 150 for this technology. The low Q_U is mainly due to the field distribution of the microstrip mode, and the very small thickness of printed resonators.

Alternative hybrid technologies are the substrate integrated waveguide (SIW) [7], [8], Empty SIW (ESIW) [9], Quarter Mode SIW (QMSIW) [10] or Air Filled SIW (ASIW) [11]. Using this family of substrate integrate technology, the Q_U is increased with respect to microstrip technology while the reduced dimensions are still maintained. Thus, this technology represents a good trade-off between volume and Q_U. For instance, in [8], the achievable Q_U is around 640 for a $FBW = 16.5\%$. The main disadvantage of this technology is the transition to other planar technologies. In SIW filters, loss performance is also sacrificed at the expense of compactness.

In applications where higher Q_U and robustness are strictly required, other non-planar alternatives, such as dielectric resonators [12], [13] or waveguide technology [14], [15] can be used. However, the compactness and low-cost manufacturing features of planar technologies are compromised.

In [12], the authors proposed the use of high dielectric constant strip resonators deposited on a low permittivity substrate. Using these dielectric resonators, filters with $Q_U \approx 880$ were demonstrated. As observed, the achieved Q_U using this technology is higher as compared to the traditional microstrip or SIW technologies (see [12]). However, in that work a standard tapped feeding line was employed to implement the I/O couplings. Due to this arrangement, rather low I/O coupling values could be implemented [12], resulting into a fractional bandwidth of only $FBW = 3.3\%$. Higher Q_U can be achieved using dielectric resonators in waveguide technology as in [13]. In [13], the fractional bandwidth is also $FBW \approx 3\%$ but with a higher quality factor of $Q_U \approx 1750$. However, the footprint is increased in comparison to the solution in [12].

Instead, using directly waveguide resonators the achievable fractional bandwidths can be increased as compared to the previous technologies (typically less than 20%), as it was for instance reported in [14]. However, much higher Q_U are possible in waveguide technology. For instance, in [15] measurements demonstrate an unloaded quality factor around $Q_U = 2700$ and a fractional bandwidth of $FBW = 8.3\%$. Even though compact solutions have been proposed [15], the sizes of waveguide filters are normally higher than with other implementations using planar or hybrid technologies.

In this context, we present in this work an alternative technology to realize wideband filters with reduced footprints in comparison to waveguide and dielectric resonator technologies, while maintaining large Q_U as compared to planar technologies. A 3D view of the proposed technology is shown in Fig. 1.

The proposed technology employs thick half-wavelength metallic bars buried in a dielectric medium. A metallic enclosure is employed to avoid spurious radiation (see Fig. 1). In comparison to planar technologies, we will demonstrate that the thick bars significantly increase the achievable coupling levels among resonators, while providing larger Q_U. The use of metallic bars with large thickness also produces a strong decrease in the characteristic impedance of the guided TEM mode. Consequently, we demonstrate that I/O couplings can be implemented by introducing a step impedance discontinuity between the coaxial connectors and the first/last resonators. In this way, explicit I/O feeding lines are avoided. The adjustment of this step impedance discontinuity together with the capability to implement very large inter-resonator couplings, will enable to implement wideband frequency responses. Since no I/O lines are required, the footprint of the structure is reduced as compared to standard boxed microstrip printed technology and SIW. However, the manufacturing complexity and volume are increased with respect to these strictly planar technologies.

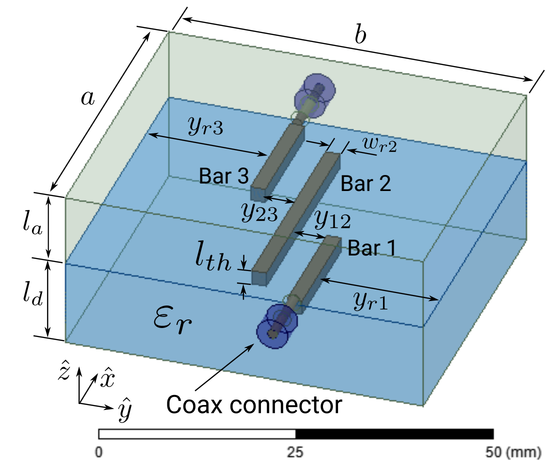

FIGURE 1. 3D view of the proposed filter technology based on bulky bars buried in a dielectric medium. The sketch shows an example of a filter using three bar resonators enclosed in a house cavity. I/O couplings are implemented with the step impedance discontinuity produced from a direct connection of the coaxial connectors with the first/last bar resonators.

In comparison to non-planar technologies, thick bar resonators exhibit Q_Us that are similar than the ones obtained using dielectric resonators, but lower than waveguide resonators. However, the I/O mechanism proposed in this paper together with the high inter-resonator couplings achievable with the thick bars allow to increase the achievable fractional bandwidths. The manufacturing complexity is similar to these non-planar technologies, while the weight, footprint and volume are significantly reduced.

In this paper we also show that an additional resonant mode can be excited in the shielding cavity partially filled with dielectric, similar to the idea proposed in [16], [17]. In those works, the I/O feeding lines were used to excite an additional cavity box resonance. In this new structure, some of the bar resonators, when adequately placed inside the cavity, can conveniently couple to this additional resonant

This work is licensed under a Creative Commons Attribution 4.0 License. For more information, see https://creativecommons.org/licenses/by/4.0/.

mode. This will allow for the implementation of transversal topologies [18], which can be used to produce transmission zeros at finite frequencies in the insertion loss response of the filter.

To demonstrate these features, three filters are designed using the proposed concept. First, a third order in-line filter is designed using only three thick bar resonators (not using the cavity mode). The filter is designed at C-band, with center frequency $f_{c1} = 4.26$ GHz, and bandwidth $BW_1 = 800$ MHz, leading to fractional bandwidth of $FBW_1 = 18.78\%$. Then, a transversal-based topology of order four is implemented with three bar resonators and one box resonator. The transversal filters are also designed at C-band, with center frequencies $f_{c2} = 3.26$ GHz and $f_{c3} = 3.35$ GHz, and bandwidths $BW_2 = 1.15$ GHz and $BW_3 = 1.575$ GHz, leading to fractional bandwidths of $FBW_2 = 35.28\%$ and $FBW_3 = 47.01\%$, respectively.

To validate the new concept, the first transversal filter with lower bandwidth (BW_2) has been manufactured using thick bars made of copper, and Teflon as the dielectric material. The external housing is made from aluminum. Measurements obtained from the manufactured hardware show very good agreement against initial target specifications, and with respect to full-wave simulations obtained with Ansys High-Frequency Structure Simulator (HFSS) [19]. The results demonstrate that the technology proposed in this contribution represents a good trade-off between high performance (in terms of IL, RL and Q_U) and compactness, allowing the implementation of very wideband responses, and with good spurious free range (SFR) performance.

II. THICK BAR TECHNOLOGY CHARACTERIZATION

In this section, we first characterize the proposed technology in terms of the resonators Q_U (subsection II-A), inter-resonator couplings (subsection II-B) and input/output couplings (subsection II-C). Special attention will be given to the effect of the metallization thickness in these parameters, since this is the distinct feature as related to standard planar technologies.

A. QUALITY FACTOR OF RESONATORS

The proposed technology is first characterized in terms of achievable Q_U, by using one isolated metallic bulky bar acting as a microwave resonator (see inset of Fig. 2). The behavior of the resonator according to its length (l_r) and width (w_{r2}, see Fig. 1) is similar to a microstrip resonator. However, in contrast to printed microstrip resonators, the proposed technology uses bars with a non negligible thickness (l_{th}, see Fig. 1). Due to this reason, in Fig. 2 we plot the value of Q_U for different thickness of the resonator l_{th} (0.1 mm $< l_{th} <$ 5 mm). The bar resonator is made of copper with conductivity $\sigma_c = 5.8 \cdot 10^7$ S/m, and it is placed above a dielectric medium made of Teflon ($\epsilon_r = 2.1$, $\tan\delta = 0.001$) with thickness $l_d = 10$ mm. All the elements are placed inside a cavity made of aluminum with conductivity $\sigma_b = 3.8 \cdot 10^7$ S/m.

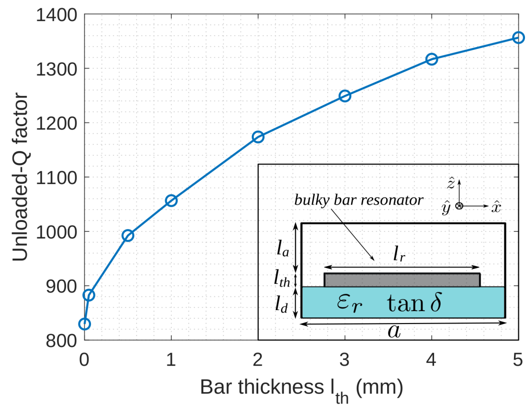

FIGURE 2. Unloaded quality factor (Q_U) of a single bulky bar resonator, as a function of the thickness (l_{th}). The geometry under test is shown in the inset. The dielectric is Teflon with a relative permittivity of $\epsilon_r = 2.1$ and a loss tangent $\tan\delta = 0.001$. The bar is made using copper with conductivity $\sigma_c = 5.8 \cdot 10^7$ S/m, and the box is made of aluminum with conductivity $\sigma_b = 3.8 \cdot 10^7$ S/m. Other dimensions are $l_d = 10$ mm, $l_a = 10$ mm, $l_r = 15$ mm, $w_r = 2$ mm (bar resonator width in the $\hat{y}$ axis), $a = 30$ mm and $b = 20$ mm (box dimension in the $\hat{y}$ axis). The test frequency is $f_c = 5.56$ GHz.

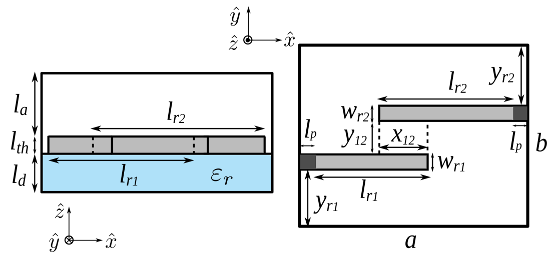

FIGURE 3. Side (left panel) and top (right panel) view of two coupled thick bar resonators, showing relevant dimensions. Feeding ports are shown with dark areas l_p.

According to Fig. 2, results show a strong dependence of Q_U with the resonator thickness l_{th}. Maximum Q_U of 1360 is obtained for the largest thickness $l_{th} = 5$ mm. This value drops to $Q_U = 830$ for the thinnest considered metalization of $l_{th} = 0.1$ mm. This study, therefore, shows the first benefit of the proposed technology, namely, the possibility of having significantly larger Q_U values as compared to those obtained using printed resonators. This large Q_U can be attributed to the extended metallic surface provided by the bulky bars, through which the induced currents can flow.

B. INTER-RESONATOR COUPLINGS

The next step is to characterize the inter-resonator coupling when the bulky bar technology is used. For this purpose, let us consider two symmetric coupled resonators as illustrated in Fig. 3. The dark areas in this figure l_p represent the feeding ports of the resonators. With this setup, we calculate a normalized inter-resonator coupling coefficient M_{ij} between the two resonators, using the described frequency plan for the

This work is licensed under a Creative Commons Attribution 4.0 License. For more information, see https://creativecommons.org/licenses/by/4.0/.

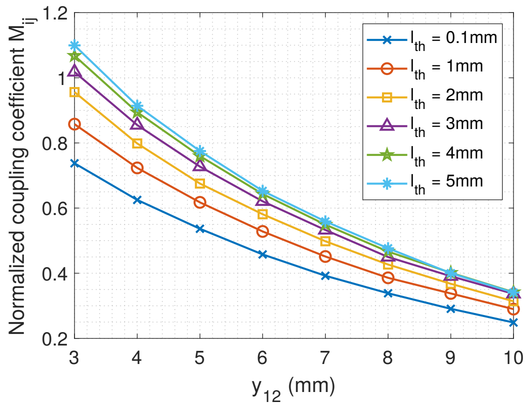

FIGURE 4. Normalized coupling coefficient as a function of the separation between resonators y_{12}, for various bar thicknesses l_{th}. Coupling coefficient is normalized with the first frequency plan ($f_{c2} = 3.26$ GHz, $BW_2 = 1.15$ GHz, $FBW_2 = 35.28\%$). Other dimensions are: $a = 30$ mm, $b = 28$ mm, $y_{r1} = y_{r2} = 10$ mm, $w_{r1} = w_{r2} = 2$ mm, $x_{12} = 0$ mm, $l_d = 10$ mm, $l_a = 10$ mm, $\varepsilon_r = 2.1$.

bandwidth BW_2 [2]

$$M_{ij} = \frac{f_{c2}}{BW_2} k_{ij} \tag{1}$$

where k_{ij} is the inter-resonator coupling coefficient extracted from the even/odd frequencies of the two coupled resonators. As usual, the test is done under very weak I/O couplings.

In Fig. 4, the normalized coupling coefficient M_{ij} is shown as a function of the separation between bars y_{12}, and for different thicknesses l_{th}. Similarly to two coupled microstrip printed resonators, the inter-resonator coupling in this structure can be controlled using both y_{12} and the overlapping distance along the $\hat{x}$-axis (x_{12}, see Fig. 3). This is observed in the plot, since the normalized coupling coefficient clearly increases as y_{12} is decreased. What it is more interesting is the behavior of the inter-resonator coupling with the bar thickness. The plot clearly indicates that the inter-resonator coupling can be significantly increased using thick bars. In particular, if the thickness of the bar resonator is small ($l_{th} = 0.1$ mm), the maximum normalized coupling value is $M_{ij} = 0.78$. This coupling can be increased to $M_{ij} = 1.15$ if l_{th} is increased to 5 mm. This study shows the second benefit of the proposed technology, which is the possibility to obtain larger inter-resonator couplings. They can be attributed to a stronger capacitive effect that is formed between bars, when the thickness is increased.

C. INPUT/OUTPUT COUPLINGS

The implementation of wideband responses requires not only of large inter-resonator couplings, but also a mechanism to implement large I/O couplings. In this context, it is important to mention that another difference between the proposed technology and traditional microstrip implementations is the characteristic impedance of the transmission line (TEM) mode, formed by the thick bar structure. In general, microstrip filters are designed with standard coaxial transitions with $50\,\Omega$ or $75\,\Omega$ transmission line impedances. The microstrip line is usually dimensioned to match the coaxial impedance, in order to avoid unnecessary reflections between the first/last printed lines and the source/load. Since no impedance mismatch is introduced, the first/last metalizations in these structures act as the feeding lines for the printed coupled-line resonators of the filter [1]. However, when the thickness of the metalization increases, the characteristic impedance substantially drops. Consequently, large impedance mismatch can be introduced between the coaxial connectors and the thick bar acting as a transmission line.

The idea proposed in this contribution is to implement the I/O couplings of the filter by directly using this impedance mismatch. Following this idea, the feeding lines traditionally used in regular printed microstrip filters are eliminated. The I/O couplings are simply implemented by the step impedance discontinuity introduced when directly connecting the pin of the coaxial connector to the first/last thick bar resonators (represented with dark areas l_p in Fig. 3). On this basis, the third advantage of the proposed technology is reduced footprint in comparison to non-planar technologies but also to regular boxed microstrip filters (that requires two additional I/O feeding lines).

To illustrate the concept, a test with a singly loaded resonator is performed to obtain the external quality factor Q_{ext} as a function of the characteristic impedance Z_p of the input coaxial connector, modeled as a lumped port connected to the thick bar resonator. The structure employed for this test is depicted in the inset of Fig. 5. The test is performed by computing the maximum value of the group delay for the S_{11} parameter in this singly terminated configuration [2]. Results are presented in Fig. 5 as a function of the port reference impedance Z_p for different bar thickness l_{th}. The values obtained for small port impedances are around $Q_{ext} = 70 - 100$, while $Z_p > 10\,\Omega$ produce very low external quality factors ($Q_{ext} < 10$). We can also observe that, when Z_p is small, the use of thicker bars leads to smaller Q_{ext}. For instance, the largest Q_{ext} is around 100 when l_{th} is small ($l_{th} = 1$ mm). This value decreases to 70 if a thicker bar is used ($l_{th} = 5$ mm). However, the effect of the thickness in the Q_{ext} is marginal when $Z_p > 10\,\Omega$.

The observed behavior indicates that very large I/O couplings are indeed achievable by properly adjusting the step impedance discontinuity introduced between the coaxial connector and the first/last resonator, and therefore there is no need to use extra I/O feeding lines. The opportunity to implement very large I/O couplings, finally demonstrates another benefit of the proposed technology, which is the possibility to synthesize very wideband responses.

III. DESIGN OF FILTERS BASED ON THICK BAR TECHNOLOGY

In this section, an in-line filter and two additional filters implementing a transversal topology are desgined using the proposed thick bar resonator technology.

This work is licensed under a Creative Commons Attribution 4.0 License. For more information, see https://creativecommons.org/licenses/by/4.0/.

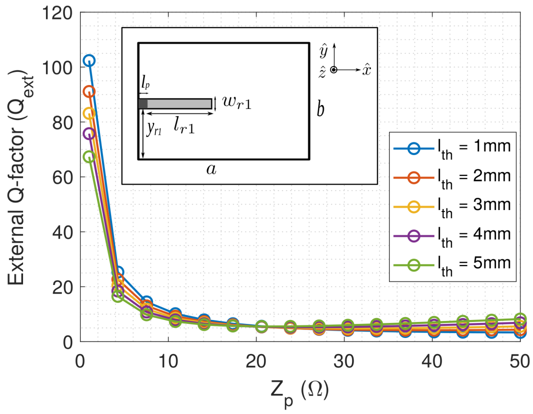

FIGURE 5. External quality factor Q_{ext} as a function of the input port reference impedance Z_p, for various values of the bar thickness l_{th}. The test frequency is $f_c = 3.5$ GHz. Other dimensions are: $l_d = 10$ mm, $l_a = 10$ mm, $y_{r1} = 10$ mm, $w_{r1} = 2$ mm, $a = 38$ mm, $b = 32$ mm. The dark area l_p denotes a lumped port that models the direct connection of the coaxial pin to the resonator.

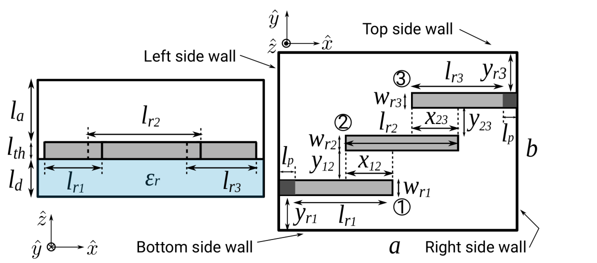

FIGURE 6. Top (right panel) and side (left panel) view of the three filters designed using the new proposed technology (one following the in-line topology and two more with a transversal topology). Relevant dimensions are also shown. Thick bars are identified with numbers. For the transversal filters the bars are numbered according to resonators shown in the coupling topology of Fig. 9. Dark areas (l_p) represent lumped ports that model the direct connection of the coaxial pins to the first/last resonators.

A. IN-LINE FILTER

To demonstrate the feasibility of the described technology, the design of a three order filter is presented in this subsection, using the classical in-line topology. The filter is centered at $f_{c1} = 4.26$ GHz, and has a bandwidth of $BW_1 = 800$ MHz ($FBW_1 = 18.78\%$). The structure of the filter is presented in Fig. 1. It will incorporate three thick bar resonators with the geometry sketched in Fig. 6. The three bars represent the resonators of the filter. In Fig. 6, the first and the third bars are coupled by proximity to the second bar resonator placed at the center of the box (bar 2). For the practical realization of the structure, the three thick bar resonators are buried in a dielectric material of height l_d. To avoid the excitation of box modes, a foam substrate with $\epsilon_r = 1.07$ has been used in this design. It should be remarked that the previously described mechanism for the I/O ports is used in this design. This is the reason why we cannot see extra I/O feeding lines in the structure shown in Fig. 6.

The $(N+2)$ coupling matrix of the designed in-line filter for a transfer function with return losses $RL = 20$ dB is [2]

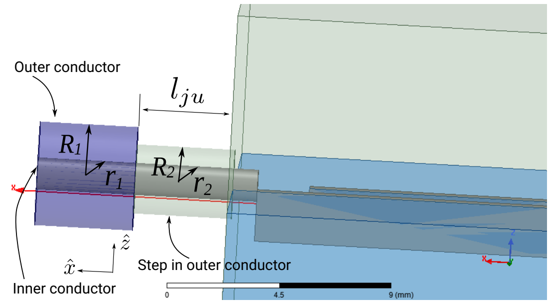

FIGURE 7. 3D view of the coaxial transition employed to adjust the I/O couplings.

$$M = \begin{bmatrix} 0 & 1.082 & 0 & 0 & 0 \\ 1.082 & 0 & 1.03 & 0 & 0 \\ 0 & 1.03 & 0 & 1.03 & 0 \\ 0 & 0 & 1.03 & 0 & 1.082 \\ 0 & 0 & 0 & 1.082 & 0 \end{bmatrix} \tag{2}$$

First, the I/O coupling ($M_{S1} = M_{3L} = 1.082$) can be adjusted with the external quality factor Q_{ext}, which can be computed from the normalized I/O coupling as [2]

$$Q_{ext} = \frac{f_{c1}}{M_{S1}^2\, BW_1} \tag{3}$$

leading to $Q_{ext} = 4.548$. From this expression it can be observed that wide bandwidths lead to small values of Q_{ext}, thus requiring large I/O couplings. However, these large couplings can be implemented by adjusting the step impedance discontinuity between the coaxial pin and the first/last bar resonator. In fact, the plot shown in Fig. 5 indicates that the required value of Q_{ext} is about the minimum values that can be obtained with the proposed I/O coupling mechanism.

In order to employ a commercial I/O connector, and at the same time permitting the implementation of the required Q_{ext} value, we propose to introduce a step discontinuity in the radius of a standard coaxial connector. Details of the arrangement are shown in Fig. 7. The nominal radii of the inner and outer conductors of the connector are R_1 and r_1 respectively, giving a characteristic impedance of 50 Ω. Next, a length l_{ju} is reserved in the cavity wall to introduce a step discontinuity in these radii. The internal conductor radius is provided by the commercial connector, and therefore it is easier to leave it untouched ($r_2 = r_1$). In order to lower the characteristic impedance of the coax, a step discontinuity is introduced in the radius of the outer conductor R_2. By selecting $R_2 < R_1$ and $r_2 = r_1$ (see Fig. 7), the characteristic impedance of the corresponding section can be substantially lowered.

For the implementation of the required I/O couplings, the commercial connector PE4128 from PASTERNACK was selected for the external section shown in Fig. 7, leading to outer and inner conductors radii of $R_1 = 2.1$ mm and $r_1 = 0.65$ mm. As mentioned before, the internal section that implements the step discontinuity takes the same radius

This work is licensed under a Creative Commons Attribution 4.0 License. For more information, see https://creativecommons.org/licenses/by/4.0/.

TABLE 1. Physical dimensions of the designed third order in-line filter, according to the sketches shown in Fig. 6 and Fig. 7, with foam as a dielectric material ($\varepsilon_r = 1.07$).

Parameters of the filter	Dimensions (in mm) In-line filter
l_a	8
l_d	6
l_{th}	2
$l_{r1} = l_{r3}$	16.35
l_{r2}	29.09
$w_{r1} = w_{r2} = w_{r3}$	2
$y_{r1} = y_{r3}$	5.1
$y_{12} = y_{23}$	5.1
$x_{12} = x_{23}$	13.9
R_1	2.1
R_2	0.9
$r_1 = r_2$	0.65
l_{ju}	4
a	35.99
b	26.2

for the inner conductor ($r_2 = r_1$), while it changes the radius of the outer conductor to $R_2 = 0.9$ mm. This example shows the high flexibility of the proposed technique to obtain very large I/O couplings, while employing commercial $50\,\Omega$ I/O coaxial connectors.

Once the I/O couplings are implemented, the next challenge is to implement the required normalized inter-resonator couplings ($M_{12} = M_{23} = 1.03$). Equation (1) clearly indicates that wide bandwidths again require very large inter-resonator couplings ($k_{12} = k_{23}$). This large couplings can be implemented by increasing the thickness of the bars, as detailed in the previous section. Once a proper thickness value is selected for the bar resonators, the inter-resonator coupling can be fine adjusted by acting on the variables $x_{12} = x_{23}$ and $y_{12} = y_{23}$ of Fig. 6. This is easily accomplished by producing charts similar to the one shown in Fig. 4.

At this point we should stress that the design of filters using this coupling matrix approach is only accurate for narrow band filters. This is because of the intrinsic narrow band approximation implied in deriving the equivalent circuit represented by the coupling matrix (based on lumped elements and ideally constant impedance or admittance inverters). Due to dispersive effects in the elements of the real physical implementation, a final optimization step is needed to recover the desired target specifications. After this optimization step, the final dimensions of the designed filter are collected in Table 1. The total size of the filter is 35.99 mm $\times$ 26.2 mm $\times$ 16 mm.

The in-band response of the in-line filter is shown in Fig. 8. The full-wave response of the filter is compared to the coupling matrix response, showing that the design process is effective for the presented filter. It can be observed very good agreement between the full-wave response and the circuit model inside the passband. In particular, the right center frequency, bandwidth and return loss levels have been correctly recovered. Out of the passband, the rejection slopes between the full-wave response and the circuit model

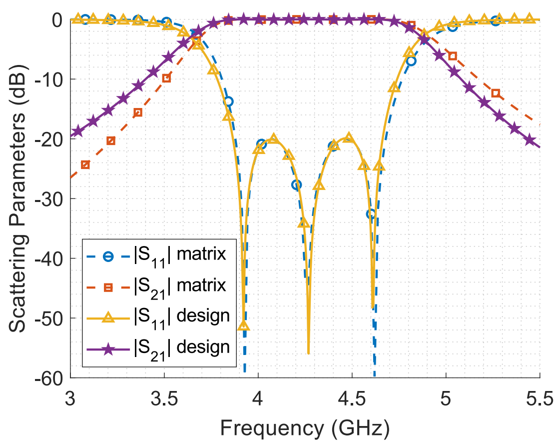

FIGURE 8. Scattering parameters of the in-line filter obtained with HFSS (design) and compared to the coupling matrix response (matrix). The bandwidth is $BW_1 = 800$ MHz ($FBW_1 = 18.78\%$). The dimensions are reported in Table 1.

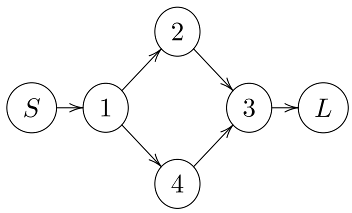

FIGURE 9. Coupling topology that represents the filter structure shown in Fig. 6, with an additional cavity resonance. Bar resonators correspond to resonators 1, 2, and 3 in this topology, while the cavity resonance is represented by resonator 4. Input and output ports are denoted as source (S) and load (L), respectively. Couplings are shown with arrows.

start to differ from each other. Again, this is due to the large bandwidth of the filter, that introduces, in the physical implementation, important dispersion effects in resonators and coupling elements. However, as observed in Fig. 8, the optimization process can effectively compensate for these effects to correctly recover the response inside the bandwidth.

B. TRANSVERSAL FILTERS

In this subsection, we address the design of two fourth order transversal filters with two different bandwidths. The first design ($f_{c2} = 3.26$ GHz, $BW_2 = 1.15$ GHz) has a prescribed transmission zero at $f_{z2} = 4.15$ GHz, while the second design ($f_{c3} = 3.35$ GHz, $BW_3 = 1.575$ GHz) has a prescribed transmission zero at $f_{z3} = 4.5$ GHz. The positions of the transmission zeros have been adjusted to achieve a ripple level of approximately 20 dB in the rejection band. Note that both filters have quite large fractional bandwidths ($FBW_2 = 35.28\%$ and $FBW_3 = 47.01\%$).

The 3D structure to be designed can be seen in Fig. 1. It will incorporate three thick bar resonators with the geometry sketched again in Fig. 6. As before, the three thick bar resonators are buried in the dielectric material. The main difference with respect to the filter designed in the previous subsection is that now the dielectric material that partially

This work is licensed under a Creative Commons Attribution 4.0 License. For more information, see https://creativecommons.org/licenses/by/4.0/.

fills the cavity is Teflon, and this allows the excitation of an additional box resonance (as described in [16], [17]). This box resonance will form the fourth resonator of our fourth order filter structure. The first/last bar resonators (bars 1 and 3 in Fig. 6) placed close to the left/right side walls of the cavity will couple to this resonance. On the contrary, the thick bar placed at the center (bar 2 in Fig. 6), will barely couple to this mode [16]. As a result, the coupling topology implemented with this arrangement is of the type known as transversal [20], and it is illustrated in Fig. 9. This coupling topology can implement one transmission zero at finite frequencies [20].

The $(N+2)$ coupling matrix of the designed filters for a transfer function with return losses $RL = 20$ dB is [2]

$$M_1 = \begin{bmatrix} 0 & 1.03 & 0 & 0 & 0 & 0 \\ 1.03 & 0.07 & 0.816 & 0 & -0.402 & 0 \\ 0 & 0.816 & 0.378 & 0.816 & 0 & 0 \\ 0 & 0 & 0.816 & 0.07 & 0.402 & 1.03 \\ 0 & -0.402 & 0 & 0.402 & -0.949 & 0 \\ 0 & 0 & 0 & 1.03 & 0 & 0 \end{bmatrix} \tag{4}$$

The implementation of the input/output couplings as well as the couplings between bars can be accomplished by following similar considerations described in subsection III-A.

From the matrix shown in (4), we can see that, in this case, one of the four inter-resonator couplings must have negative sign, necessary for implementing single-band responses. This is given by the elements $M_{14} = -M_{34}$, representing the couplings between the first/last (1,3) bars and the cavity resonance. To implement this sign change, bars 1 and 3 are located at opposite side walls of the cavity (left and right side walls as shown in Fig. 6). The sign change is finally produced by a direction inversion in the electric field of the box mode when going from the left to the right side walls of the cavity. More details about the field distribution of this mode are given in [16]. The absolute value of this coupling will be dependent on the distance from these bars to the top and bottom sidewalls (parameter $y_{r1} = y_{r3}$ in Fig. 6), as well as on the air and dielectric heights (parameters l_a and l_d in Fig. 6). Since the $\hat{x}$-component of the electric field is zero at the top/bottom side walls, this coupling increases when y_{r1} and y_{r3} increase.

The third filter requires a stronger coupling since it has a wider bandwidth (BW_3). This is achieved by increasing $y_{r1} = y_{r3}$. However, this distance also affects the width of the box b, therefore modifying the resonant frequency of the cavity mode (M_{44} of the coupling matrix). To correct for this shift of the resonant frequency, the overlapping distance between bars $x_{12} = x_{23}$ can be shortened, thus effectively decreasing the length of the box a. Alternatively, the resonant frequency of the cavity mode can also be adjusted by modifying the air and/or dielectric heights, l_a and l_d. We note that the modification of the overlapping distance $x_{12} = x_{23}$ will, in turn, change the couplings between bars $M_{12} = M_{24}$. However, the effect is compensated, once more, with the adjustment of the separation between them $y_{12} = y_{23}$. After all couplings and resonant frequencies are adjusted, a global

TABLE 2. Physical dimensions of the two transversal filters designed in this paper, according to the sketches shown in Fig. 6 and Fig. 7, with Teflon as dielectric material ($\varepsilon_r = 2.1$).

Parameters of the filter	Dimensions (in mm) Second design ($BW_2 = 1.15$ GHz)	Dimensions (in mm) Third design ($BW_3 = 1.57$ GHz)
l_a	10	8
l_d	10	8
l_{th}	2	2
$l_{r1} = l_{r3}$	16.1	15.98
l_{r2}	30.2	26.6
$w_{r1} = w_{r2} = w_{r3}$	2	2
$y_{r1} = y_{r3}$	16.8	19.3
$y_{12} = y_{23}$	4.5	3.2
$x_{12} = x_{23}$	11.1	13.9
R_1	2.1	2.1
R_2	1.2	1.4
$r_1 = r_2$	0.65	0.65
l_{ju}	4	4
a	42.2	32.76
b	48.6	51

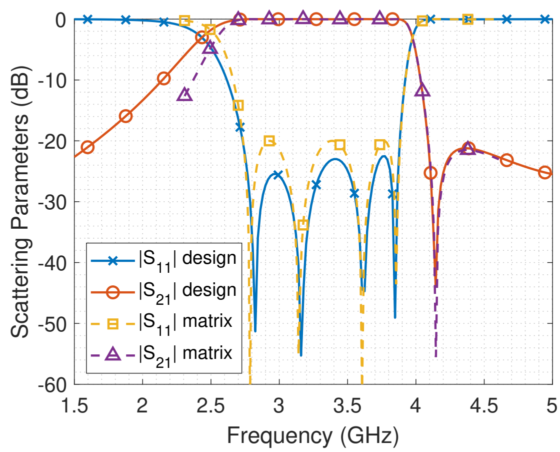

FIGURE 10. Scattering parameters of the second designed filter obtained with HFSS (design) and comparison to the coupling matrix response (matrix). The bandwidth is $BW_2 = 1.15$ GHz ($FBW_2 = 35.28\%$). The dimensions of this second design are reported in the second column of Table 2.

optimization is applied to the whole structure for fine tuning. Again, this is mainly needed due to the large bandwidths of the implemented filters, that require for the compensation of the dispersive behavior of the filter elements. After this final optimization step, the final dimensions of the two designed filters are included in Table 2. The total size of the two transversal filters are 42.2 mm × 48.6 mm × 12 mm (for the second design) and 32.76 mm × 51 mm × 18 mm (for the third design).

Details of the in-band responses for the two designed filters are shown in Fig. 10 and Fig. 11. Comparisons with respect to the responses of the coupling matrix are also included, showing that the design process was effective for both filters. In the two examples the transmission zero is placed approximately at the same distance from the passband edge, thus demonstrating that the passband characteristics can be controlled with the proposed structure, independently from the position of the transmission zero. As observed from

This work is licensed under a Creative Commons Attribution 4.0 License. For more information, see https://creativecommons.org/licenses/by/4.0/.

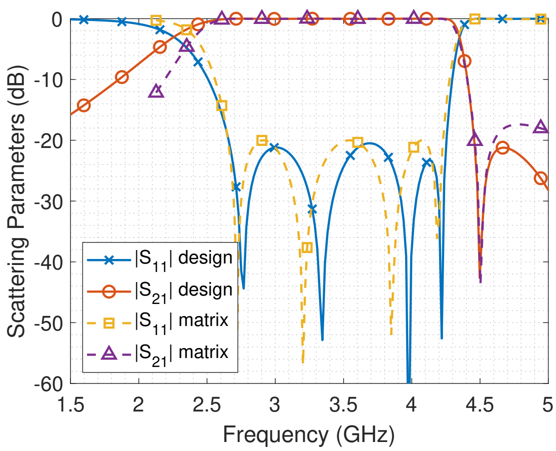

FIGURE 11. Scattering parameters of the third designed filter obtained with HFSS (design) and comparison to the coupling matrix response (matrix). The bandwidth is $BW_3 = 1.57$ GHz ($FBW_3 = 47.01\%$). The dimensions of this third design are reported in the third column of Table 2.

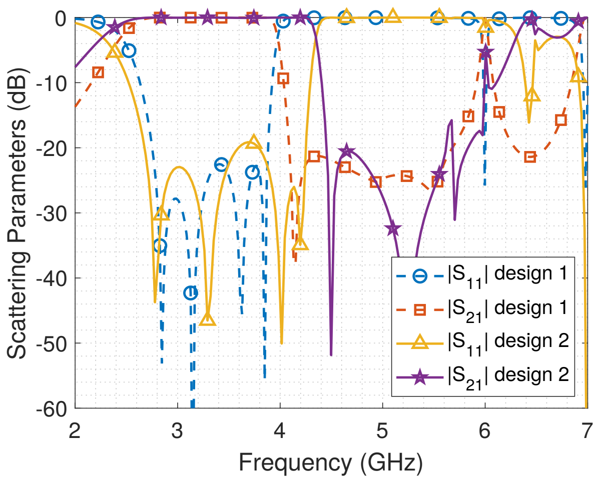

FIGURE 12. Comparison for the out of band responses of the two last designed transversal filters from HFSS simulations. Dimensions of both filters are collected in Table 2.

Fig. 10 and Fig. 11, the transmission zero appears above the passband. However, by swapping the resonant frequencies of the resonators 2 and 4 (see Fig. 9), the transmission zero can be shifted bellow the passband (this is known in the scientific literature as the zero shifting property).

To conclude, a comparison between the two last filters in terms of spurious free range (SFR) has been performed. The out of band responses of both filters are compared in Fig. 12. As it can be observed, the SFR of the two filters is similar. In both cases, the first spurious band appears at $f_{s1} = 6$ GHz, and is due to the excitation of higher order resonances in the shielding cavity. This gives $SFR_2 \approx 2.1$ GHz (54 %) for the second filter and $SFR_3 \approx 1.8$ GHz (43 %) for the third design.

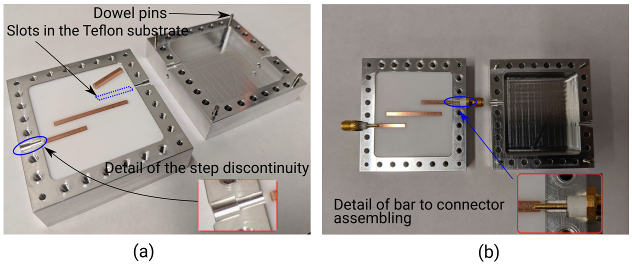

FIGURE 13. Manufactured prototype. (a) Components of the filter before assembling, and details of the slots in the Teflon substrate used for alignment. The inset inside shows the step discontinuity needed in the radius of the outer conductor for the I/O coupling adjustment. (b) Top view of the structure after assembling. Inset shows details of the assembling process between the coax center pin and the copper bar.

IV. PROTOTYPE MANUFACTURING AND MEASUREMENTS

The first transversal filter designed in the previous section (second design) has been manufactured and measured. A photograph of the prototype is presented in Fig. 13. Details of one of the copper thick bars, before assembling, can be observed in Fig. 13(a). As shown, the thick bars are buried into slots mechanized in the Teflon substrate. The bars have been manufactured using a traditional milling process. The aluminium enclosure used for shielding is manufactured in two pieces that are aligned using four dowel pins (see Fig. 13(a)). This allows to easily mechanize in the left/right side walls of the cavity the step discontinuities required in the radius of the outer conductor for the I/O coupling adjustment. A detail of this process in shown in the inset of Fig. 13(a). Details of the assembling process of the connector pins with the copper bars are shown in the inset of Fig. 13(b). The two pieces of the enclosure are finally assembled with the use of 24 pressure screws. Rounded corners of 2 mm are introduced in the different parts of the structure, as required by the milling process. They have shown to have little effect on the electrical behavior of the filter.

Measurements corresponding to the prototype in Fig. 13 are compared to the in-band full-wave response obtained using HFSS in Fig. 14. As can be observed, the in-band measured response shows good agreement with respect to the full-wave simulation, thus fully validating the proposed concept. The small differences could be due to manufacturing issues and losses in real components.

From the obtained results we can see that the transmission zero is slightly closer to the passband than expected. This raises the stopband ripple from 20 dB to 16 dB. Moreover, the measured bandwidth is $BW = 1.06$ GHz being slightly smaller than the target value. This finally leads to a measured fractional bandwidth of 32%. Note that this large bandwidth is difficult to achieve using planar technologies based on resonant elements and even with dielectric or waveguide resonators.

As observed in Fig. 14, the return loss level is around 20 dB. We note that two poles of the transfer function are complex due to manufacturing errors and imprecisions dur-

This work is licensed under a Creative Commons Attribution 4.0 License. For more information, see https://creativecommons.org/licenses/by/4.0/.

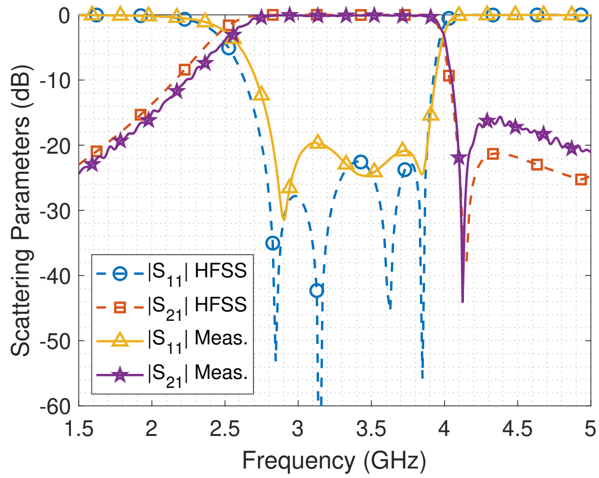

FIGURE 14. Comparison between the S-parameters simulated using the full-wave commercial software HFSS and measured data from the manufactured prototype shown in Fig. 13.

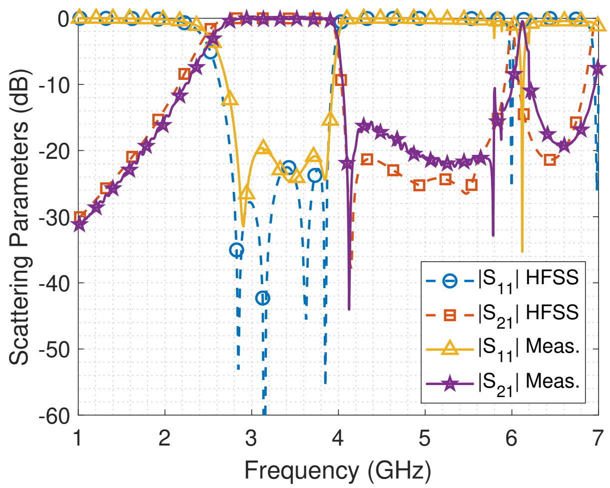

FIGURE 15. Comparison between the S-parameters simulated using the full-wave commercial software HFSS and measured data from the manufactured prototype shown in Fig. 13 (out of band performance).

ing the assembling process. It should be emphasized that the presented results are obtained directly from the manufactured prototype without applying any post-tuning operation. The insertion of tuning elements in this filter would complicate the manufacturing process. Furthermore, the measured insertion losses are $IL = 0.16$ dB. This corresponds to an approximate value for the unloaded quality factor of $Q_U = 1180$.

Finally, we check the measured out of band response for the manufactured prototype and compare it to full-wave simulations in Fig. 15. Good agreement between measured results and the ideal response is also achieved in this case. These results experimentally confirm that the first spurious band appears at $f_{s1} = 6$ GHz, confirming a $SFR \approx 2.1$ GHz (54%). This performance is also good as compared to other transversal filters implementations previously reported. See for instance the transversal filter implemented in waveguide technology with $SFR = 21\%$, reported in [18].

In Table 3, we compare the proposed solution to other resonant filters reported in the technical literature, in terms of Q_U, FBW, electrical size and IL. As observed in Table 3, the obtained Q_U value is greater than values typically reported for microstrip technology ($Q_U < 150$) and SIW technology ($Q_U < 640$) [6], [8]. This is achieved at the expense of a higher volume of the filter. However, the footprint does not increase significantly, since no I/O feeding lines are required. This filter also has a higher Q_U than the filter based on dielectric resonators proposed in [12], where a $Q_U = 880$ was reported. However, as expected the achieved Q_U is lower that those typically obtained using dielectric-loaded cavities [13] and waveguide technology [15]. In contrast, comparing to dielectric [21] and waveguide [15] resonators, this structure offers a more compact solution with reduced footprint and IL for wideband applications.

V. CONCLUSION

In this contribution, an alternative technology for the implementation of compact wideband filters has been proposed and experimentally validated. The advantages of thick metallic bars as microwave resonators have been verified through various examples. Such advantages include the possibility to implement wide passbands, enabled by the high couplings between thick bars. Also, input/output feeding lines are avoided by exploiting the strong mismatch between bar resonators and standard coaxial connectors. This leads to more compact structures, and allows for the implementation of very strong I/O couplings, which are also required for implementing wideband responses. Moreover, the proposed bulky resonators exhibit higher unloaded quality factors Q_U than other technologies such as microstrip or SIW. Comparing with non-planar technologies, the weight and volume is significantly reduced. Finally, we have demonstrated that the suitable excitation of an additional box resonance allows for the implementation of transversal coupling topologies. In addition to the theoretical design process, a fourth order filter with fractional bandwidth of $FBW = 32\%$ and $Q_U = 1180$, has been experimentally demonstrated. Measured return losses of 20 dB and $SFR > 50\%$ were obtained. Measurements and simulated results show good agreement, which confirm the performance of the proposed technology. The reported data experimentally validate that this technology offers good trade-off between high performance, compact size and manufacturing complexity, for filters intended for wideband communication systems.

REFERENCES

[1] J.-S. Hong, Microstrip Filters for RF/Microwave Applications. John Wiley, Sons, Inc., 2011.

[2] R. J. Cameron, C. M. Kudsia, and R. R. Mansour, Microwave Filters for Communication Systems: Fundamentals, Design and Applications. John Wiley, Sons; Inc. Hoboken, New Jersey, 2007.

[3] K. T. Jokela, "Narrow-band stripline or microstrip filters with transmission zeros at real and imaginary frequencies," IEEE Transactions on Microwave Theory and Techniques, vol. 28, no. 6, pp. 542–547, Jun 1980.

[4] D. F. Williams and S. E. Schwarz, "Design and performance of coplanar

This work is licensed under a Creative Commons Attribution 4.0 License. For more information, see https://creativecommons.org/licenses/by/4.0/.

TABLE 3. Comparison in terms of Q_U, FBW, electrical size and IL between the solution proposed in this work and other resonant filters reported in the literature.

Technology	Reference	Q_U	FBW	Electrical size	IL
Microstrip	[6]	-	10%	$0.06 \times 0.06 \times 0.0042$	1.2 dB
SIW	[8]	640	16.5%	$0.72 \times 0.72 \times 0.036$	1.5 dB
Dielectric bars	[21]	880	3.3%	$0.874 \times 0.4545 \times 0.3497$	0.6 dB
Dielectric-loaded cavities	[13]	1750	3%	$0.3438 \times 0.2865 \times 0.1719$	0.4 dB
Waveguide	[15]	2700	8.3%	$1.4 \times 1.27 \times 2.14$	0.2 dB
Thick metallic bars	**this work (second design)**	**1180**	**32%**	$\mathbf{0.464 \times 0.5347 \times 0.132}$	**0.16 dB**

waveguide bandpass filters," IEEE Transactions on Microwave Theory and Techniques, vol. 31, no. 7, pp. 558–566, Jul 1983.
[5] N. Thomson and J. Hong, "Compact ultra-wideband microstrip/coplanar waveguide bandpass filter," IEEE Microwave and Wireless Components Letters, vol. 17, no. 3, pp. 184–186, March 2007.
[6] L. Athukorala and D. Budimir, "Compact filter configurations using concentric microstrip open-loop resonators," IEEE Microwave and Wireless Components Letters, vol. 22, no. 5, pp. 245–247, May 2012.
[7] M. Bozzi, A. Georgiadis, and K. Wu, "Review of substrate-integrated waveguide circuits and antennas," IET Microwaves, Antennas Propagation, vol. 5, no. 8, pp. 909–920, June 2011.
[8] Z. Liu, G. Xiao, and L. Zhu, "Triple-mode bandpass filters on csrr-loaded substrate integrated waveguide cavities," IEEE Transactions on Components, Packaging and Manufacturing Technology, vol. 6, no. 7, pp. 1099–1105, July 2016.
[9] A. Belenguer, H. Esteban, and V. E. Boria, "Novel empty substrate integrated waveguide for high-performance microwave integrated circuits," IEEE Transactions on Microwave Theory and Techniques, vol. 62, no. 4, pp. 832–839, April 2014.
[10] S. Moscato, C. Tomassoni, M. Bozzi, and L. Perregrini, "Quarter-mode cavity filters in substrate integrated waveguide technology," IEEE Transactions on Microwave Theory and Techniques, vol. 64, no. 8, pp. 2538–2547, Aug 2016.
[11] L. Silvestri, A. Ghiotto, C. Tomassoni, M. Boziz, and L. Perregrini, "Partially air-filled substrate integrated waveguide filters with full control of transmission zeros," IEEE Transactions on Microwave Theory and Techniques, vol. 67, no. 9, pp. 3673–3682, Sep. 2019.
[12] Y. Zhu, Y. Li, and J. Chen, "A novel dielectric strip resonator filter," IEEE Microwave and Wireless Components Letters, vol. 28, no. 7, pp. 591–593, July 2018.
[13] L. Pelliccia, F. Cacciamani, C. Tomassoni, and R. Sorrentino, "Ultra-compact high-performance filters based on tm dual-mode dielectric-loaded cavities," International Journal of Microwave and Wireless Technologies, vol. 6, pp. 151–159, 04 2013.
[14] F. M. Vanin, D. Schmitt, and R. Levy, "Dimensional synthesis for wide-band waveguide filters and diplexers," IEEE Transactions on Microwave Theory and Techniques, vol. 52, no. 11, pp. 2488–2495, Nov 2004.
[15] P. Vallerotonda, L. Pelliccia, C. Tomassoni, F. Cacciamani, R. Sorrentino, J. Galdeano, and C. Ernst, "Compact waveguide bandpass filters for broad-band space applications in c and ku-bands," in 2019 European Microwave Conference in Central Europe (EuMCE), May 2019, pp. 116–119.
[16] M. Martinez-Mendoza, J. S. Gomez-Diaz, D. Canete-Rebenaque, J. L. Gomez-Tornero, and A. Alvarez-Melcon, "Design of bandpass transversal filters employing a novel hybrid structure," IEEE Transactions on Microwave Theory and Techniques, vol. 55, no. 12, pp. 2670–2678, Dec 2007.
[17] M. Martinez-Mendoza, J. S. Gomez-Diaz, D. Canete-Rebenaque, and A. Alvarez-Melcon, "Design of dual-bandpass hybrid waveguideâĂŞmicrostrip microwave filters," IEEE Transactions on Microwave Theory and Techniques, vol. 56, no. 12, pp. 2913–2920, Dec 2008.
[18] F. J. Perez Soler, M. Martinez Mendoza, F. D. Quesada Pereira, D. Canete Rebenaque, A. Alvarez Melcon, and R. J. Cameron, "Design of bandpass elliptic filters employing inductive windows and dielectric objects," IEEE Transactions on Microwave Theory and Techniques, vol. 55, no. 11, pp. 2393–2398, Nov 2007.
[19] ANSYS, High-Frequency Structure Simulator (HFSS), Release 17.2. Canonsburg, Pennsylvania (USA): ANSYS Inc., 2016. [Online]. Available: https://ansys.com
[20] S. Amari and U. Rosenberg, "The doublet: A new building block for modular design of elliptic filters," in 2002 32nd European Microwave Conference, Sept 2002, pp. 1–3.
[21] Y. Zhu, Y. Li, and J. Chen, "A novel dielectric strip resonator filter," IEEE Microwave and Wireless Components Letters, vol. 28, no. 7, pp. 591–593, July 2018.

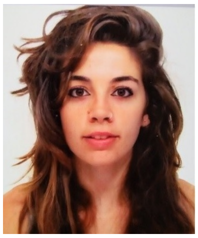

CELIA GOMEZ MOLINA was born in Murcia, Spain, in 1992. She received the degree in Telecommunication Systems from the Technical University of Cartagena (UPCT), Murcia, Spain, in 2014, and the Master's degree in Telecommunication Engineering in 2016. In 2016, she joined the Department of Information Technologies and Communications, UPCT, as a research student, where she is currently developing her teaching and research activities. She was visiting student at University of California, Davis, USA, from April 2nd, 2018 to June 22th, 2018, and at the Politecnico di Milano, Italy, from April 1nd, 2019 to June 28th, 2019. She is involved in the development of analytical and numerical tools for network representations of waveguide and planar discontinuities. Her current scientific interests also include the design of microwave filters using different technologies.

ALEJANDRO PONS ABENZA was born in Murcia, Spain, in 1990. He received the Telecommunications Systems Engineer degree from the Technical University of Cartagena (UPCT) in 2014, and the Ph. D. degree from the UPCT in 2019. In 2014, he joined the Department of Information Technologies and Communications at UPCT, as a research student. In 2016 he began a research project with the objective of developing his Ph. D. Thesis, as a collaboration between UPCT and Thales Alenia Space Spain, for the design and development of novel microwave filter structures using additive manufacturing techniques for space applications. His current research interest includes the analysis and design of microwave devices employing additive manufacturing, as well as synthesis techniques for the design of microwave filters.

This work is licensed under a Creative Commons Attribution 4.0 License. For more information, see https://creativecommons.org/licenses/by/4.0/.

JAMES DO is an RF design engineering consultant at Virginia Diodes Inc where he is designing the next generation of THz Schottky diode frequency multipliers. James completed his PhD on millimeter wave ground penetrating radar for identifying unexploded ordnance in 2019 at the University of California Davis. Previously, he was the lead RF engineer in the custom systems department at Virginia Diodes Inc. from 2008-2014 where he designed and tested systems and components operating up to 3THz including the world's first 1THz vector network analyzer extension module. During this time, he also received a Master of Electrical Engineering degree from the University of Virginia in 2013 where his research was on high directivity THz couplers.

FERNANDO QUESADA PEREIRA (S'05-M'08) was born in Murcia, Spain, in 1974. He received the Telecomunications Engineer Master degree from the Technical University of Valencia (UPV), Valencia, Spain, in 2000, and the Ph.D. degree from the Technical University of Cartagena (UPCT), Murcia, in 2007. In 1999, he joined the Radiocommunications Department, UPV, as a Research Assistant, where he was involved in the development of numerical methods for the analysis of anechoic chambers and tag antennas. In 2001, he joined the Communications and Information Technologies Department, UPCT, as a Research Assistant, and then as an Assistant Professor. In 2005, he was a Visiting Scientist with the University of Pavia, Pavia, Italy. In 2009, he was an Invited Researcher with UPV. In 2011, he became an Associate Professor with UPCT. His current research interest includes integral equation numerical methods for the analysis of antennas and microwave devices, along with microwave filters design and applications.

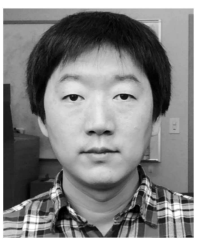

XIAOGUANG (LEO) LIU (M'10-SM'16) received the bachelor's degree from Zhejiang University, Hangzhou, China, in 2004, and the Ph.D. degree from Purdue University, West Lafayette, IN, USA, in 2010. In 2011, he joined the Department of Electrical and Computer Engineering, University of California at Davis, Davis, CA, USA, as an Assistant Professor, and was promoted to an Associate Professor in 2017. At the University of California at Davis, his research group is currently investigating various aspects of cutting-edge high-frequency and high-speed circuit and system designs.

J. SEBASTIAN GOMEZ DIAZ (M'11, SM'16) was born in Ontur, Spain. He received the MSc. and Ph.D. degrees in electrical engineering from the Technical University of Cartagena, Cartagena, Spain, in 2006 and 2011, respectively.

He is currently an Assistant Professor in the Electrical and Computer Engineering Department at the University of California, Davis. During the development of his Ph.D., he held visiting research positions with École Polytechnique de Montréal (Canada) and with the Fraunhofer Institute for High Frequency Physics and Radar Techniques (Germany). From October 2011 until March 2014, he was a postdoctoral fellow at the École Polytechnique Fédéral de Lausanne (EPFL, Switzerland). Then, from May 2014 to August 2016, he continued his postdoctoral work in the Metamaterials and Plasmonic Research Laboratory of The University of Texas at Austin. His main research interests include multidisciplinary areas of electromagnetic wave propagation and radiation, metamaterials and metasurfaces, plasmonics, 2D materials, non-reciprocal and nonlinear phenomena, and other emerging topics on applied electromagnetics and nanotechnology.

Dr. Gomez-Diaz was the recipient of a NSF CAREER Award, the 2017 Leopold Felsen Award for Excellence in Electrodynamics, the Raj Mittra Award presented by the 2015 IEEE Antennas and Propagation Society, the Young Scientist Award of the 2015 URSI Atlantic RadioScience Conference, a FP7 Marie Curie Fellowship from the European Commision in 2012, the Colegio Oficial de Ingenieros de Telecomunicación (COIT/AEIT) award to the best Spanish PhD. thesis in basic information and communication technologies in 2011, and the best Ph.D. thesis award from the Technical University of Cartagena. He serves as a reviewer for several journals on antennas, microwaves/THz and physics.

ALEJANDRO ALVAREZ MELCON (M'99-SM'07) was born in Madrid, Spain, in 1965. He received the Telecommunications Engineer degree from the Technical University of Madrid (UPM), Madrid, Spain, in 1991, and the Ph.D. degree in electrical engineering from the Swiss Federal Institute of Technology, Lausanne, Switzerland, in 1998. In 1988, he joined the Signal, Systems and Radiocommunications Department, UPM, as a research student, where he was involved in the design, testing, and measurement of broad-band spiral antennas for electromagnetic measurements support (EMS) equipment. From 1991 to 1993, he was with the Radio Frequency Systems Division, European Space Agency (ESA/ESTEC), Noordwijk, The Netherlands, where he was involved in the development of analytical and numerical tools for the study of waveguide discontinuities, planar transmission lines, and microwave filters. From 1993 to 1995, he was with the Space Division, Industry Alcatel Espacio, Madrid, Spain, and was also with the ESA, where he collaborated in several ESA/European Space Research and Technology Centre (ESTEC) contracts. From 1995 to 1999, he was with the Swiss Federal Institute of Technology, École Polytechnique Fédérale de Lausanne (EPFL), Lausanne, Switzerland, where he was involved with the field of microstrip antennas and printed circuits for space applications. In 2000, he joined the Technical University of Cartagena, Spain, where he is currently developing his teaching and research activities. Dr. Alvarez Melcón was de recipient of the Journée Internationales de Nice Sur les Antennes (JINA) Best Paper Award for the best contribution to the JINA'98 International Symposium on Antennas, and the Colegio Oficial de Ingenieros de Telecomunicación (COIT/AEIT) Award to the best Ph.D. dissertation in basic information and communication technologies. He was Invited Professor at Polytechnique University of Montreal Canada from July 1st, 2010 to September 30th, 2010, and Visiting Professor at University of California, Davis, USA, from October 2nd, 2017 to September 27th, 2018.

This work is licensed under a Creative Commons Attribution 4.0 License. For more information, see https://creativecommons.org/licenses/by/4.0/.